



HAL
open science

Effects of Zeolitic Parameters and Irradiation on the Retention Properties of Silver Zeolites Exposed to Molecular Iodine

B. Azambre, Mouheb Chebbi, Olivia Leroy, Laurent Cantrel

► **To cite this version:**

B. Azambre, Mouheb Chebbi, Olivia Leroy, Laurent Cantrel. Effects of Zeolitic Parameters and Irradiation on the Retention Properties of Silver Zeolites Exposed to Molecular Iodine. *Industrial and engineering chemistry research*, 2018, 57 (5), pp.1468-1479. 10.1021/acs.iecr.7b03579 . hal-02896997

HAL Id: hal-02896997

<https://hal.science/hal-02896997v1>

Submitted on 17 Jul 2020

HAL is a multi-disciplinary open access archive for the deposit and dissemination of scientific research documents, whether they are published or not. The documents may come from teaching and research institutions in France or abroad, or from public or private research centers.

L'archive ouverte pluridisciplinaire **HAL**, est destinée au dépôt et à la diffusion de documents scientifiques de niveau recherche, publiés ou non, émanant des établissements d'enseignement et de recherche français ou étrangers, des laboratoires publics ou privés.

Effects of Zeolitic Parameters and Irradiation on the Retention Properties of Silver Zeolites Exposed to Molecular Iodine.

Bruno Azambre^{a}, Mouheb Chebbi^{a†}, Olivia Leroy^b, Laurent Cantrel^b*

^a Laboratoire de Chimie et Physique-Approche Multi-Echelle des Milieux Complexes (LCP-A2MC- EA n°4362), Institut Jean-Barriol FR2843 CNRS, Université de Lorraine, Rue Victor Demange, 57500 Saint-Avold, France.

^b Institut de Radioprotection et de Sûreté Nucléaire (IRSN), PSN-RES, Saint-Paul Lez Durance, 13115, France.

KEYWORDS: iodine, nuclear power plant, γ -irradiation, silver zeolite, impregnation, ionic exchange, DR-UV-Vis, XRD.

ABSTRACT

In this study, we have investigated the iodine retention behavior of silver zeolite sorbents under a variety of conditions. First, a preliminary study was achieved in liquid phase in order to determine: (i) the main kinetic and thermodynamic characteristics pertaining to the adsorption behavior; (ii) the influence of some zeolitic parameters (nature of the framework, silver content,

preparation method...) on the adsorption capacities. Thanks to the on-line monitoring of gas-phase I₂ concentrations by UV-Vis spectroscopy, the iodine dynamic adsorption/desorption behavior of some selected sorbents was then studied at 100°C. It was found that faujasite sorbents with silver content higher than 20 wt% could maintain a high working capacity (up to 330 mg/g) and present a high ability for irreversible trapping. Finally, the stability of trapped iodine species was evidenced using additional tests performed at 120°C in presence of irradiation and humidity.

1. INTRODUCTION

Since the Fukushima disaster in 2011, there has been a renewed interest for the mitigation of fission products (FPs) releases in case of severe nuclear accident at short and middle terms.^{1,2} Among the different FPs, the capture of radiological iodine is of specific interest due to the high impact of the ¹³¹I and ¹²⁹I isotopes at short and long terms, respectively, and the ability of this element to exist in volatile forms.³ In the event of a core melt accident, the reactor containment might suffer damage resulting from overpressure caused by the steam inlet from the core and possible molten core concrete interactions in the containment over a long period. If the containment integrity is not maintained, significant off-site radiotoxic emissions could be released. In order to overcome this challenge, mitigation technologies such as Filtered Containment Venting Systems (FCVS)⁴ are of great interest because they can in principle prevent excessive pressures in the containment while affording simultaneously a reliable retention of radioactive products.⁵ Some FCVS already equipping nuclear containment buildings include now some filtration stages dedicated to volatile iodine. In that respect, an efficient approach may consist in combining wet or dry filtration devices (such as metallic filters, aqueous

scrubbers or sand bed filters) with an additional filter constituted by an inorganic porous adsorbent.^{6,7}

Studies focused on the investigation of nanoporous sorbents for the trapping of iodine have been increasing these last years.⁸⁻¹⁴ Among possible adsorbing materials, zeolites are obvious candidates, thanks to their thermal stability and radiation resistance, high specific surface areas, tunable pore size and chemistry¹⁵. Already in the late 70's, silver zeolites have been identified to efficiently trap molecular iodine and methyl iodide, namely thanks to the possibility of forming stable AgI precipitates (the melting point of bulk silver iodide is 558°C^{16,17}). By comparison with organic or hybrid materials such activated carbons/charcoals and Metal Organic Frameworks, silver zeolites are more robust under oxidizing/ionizing conditions.⁶ Nowadays, works are on-going to develop new FCVS with silver zeolites¹⁸ but many scientific gaps still persist, for instance about the relationships existing between the zeolite characteristics and their filtration behavior. Despite hundreds structural types of zeolites exist, most of academic and industrial studies have focused on Ag/X and Ag/MOR types.^{9,12,19-21} These latter materials are also those sold for iodine retention (FCVS and fuel reprocessing applications) by commercial suppliers (for instance under the trademark Ionex²²). Recently, we examined during systematic studies the respective influences of the zeolite framework type, the Si/Al ratio, the silver content and its speciation in the case of methyl iodide retention by silver-exchanged zeolites.^{13,14} It was found that CH₃I adsorption capacities at saturation namely depend on the silver content as dispersed Ag⁺ cations or clusters in the pores, the type of zeolitic framework having a very limited effect.¹³ However, the situation is more complex when considering important parameters, such as the useful working capacity (at breakthrough) of the sorbents or the thermal stability of trapped iodine species. In this case, exchanged faujasite Ag/Y zeolites with more than 15-20 wt% silver

were found to be much better sorbents for CH₃I capture than the other investigated materials, including those more traditionally investigated (Ag/MOR, Ag/X, Ag/FER, Ag/Beta, Ag/ZSM-5 and a commercial sorbent^{13,14}). Influential zeolitic characteristics were found to be the crystal size, the pore size, the silver and sodium contents and also the silver exchange degree. Moreover, our investigations on the CH₃I retention mechanism by the different silver zeolites also led us to conclude that both CH₃I diffusional properties and the transformation to AgI are affected by the catalytic properties of the zeolites.^{10,14} However, such information are still lacking in the case of I₂ retention and the effect of accidental conditions (irradiation, presence of other chemical species) on adsorption properties remains far to be well understood.

In the present work, we aimed to investigate the ability of well-characterized silver zeolites for the trapping of molecular iodine under different conditions, our general objective being to define the best suitable zeolite for FCVS applications. Similar sorbents than those used for CH₃I retention were studied and the effect of the preparation method (ion-exchange vs impregnation) was also considered. In a first part, a screening study on the I₂ adsorption capacities of a dozen of sorbents will be presented. Then, the retention properties of the best silver zeolites will be studied under more representative gas-phase dynamic conditions. In that respect, a totally new experimental setup was specifically designed for the determination of breakthrough and desorption profiles and related quantitative data. The possibility to continuously monitor the concentration of I₂ in the flowing gas by on-line gas-phase UV-Vis measurements during the test offers a unique possibility to overcome the limitations and uncertainties existing in most of static experiments used until now. Finally, we aimed in the last part of the paper to check iodine retention under thermal and irradiation conditions. Indeed, a good efficiency of trapping is not

sufficient from the viewpoint of nuclear safety, the retention has also to be as much irreversible as possible.

2. EXPERIMENTAL

2.1. Materials

Commercial zeolites of structural types FAU (Y, Si/Al=2.5, *CBV 300*), MOR (Si/Al = 10, *CBV21A*), FER (Si/Al = 10.5, *CP914C*), *BEA (Beta, Si/Al = 10.1, *CP814E**), MFI (ZSM-5, 11.5, *CBV 2314*) were all provided by Zeolyst in ammonium form. A 13X (NaX) zeolite (Si/Al=1.2, 60-80 mesh, *20305*) was supplied by Sigma Aldrich. Incorporation of silver was carried out either by ion-exchange or impregnation in order to tune the dispersion and speciation of silver within the obtained sorbents. In order to avoid any photo-reduction of silver species, all preparation steps and samples storage were done in the dark.

Silver-exchanged zeolites. Most of investigated sorbents were prepared by ion-exchanging the parent (commercial) zeolites with silver nitrate (Sigma-Aldrich, purity > 99.9 %). These materials are similar to those used in our previous studies related to CH₃I retention.^{13,14} Briefly, for each preparation, 2 g of zeolite were added to a 0.01M AgNO₃ solution (200 mL) at 25 °C and stirred for 24 hours. Then, the exchanged zeolites were vacuum-filtered and dried at 80°C overnight. Whenever necessary, this ion-exchange procedure was repeated up to 2 (MOR structure) or 3 times (Y, ZSM-5, and 13 X structures) in order to achieve higher exchange degrees and Ag contents. Prior to adsorption and characterization studies, all the zeolitic materials were calcined under air in a muffle furnace with a heating rate of 5°C/min from room temperature to 200°C (plateau of 1 hour) and then to 500°C (plateau of 2 hours). Exchanged-zeolites were denoted afterwards *xAg/Structure (Si/Al)* where x is the mass percentage in silver.

Impregnated zeolites. In order to study the effects of both the preparation method and the Si/Al ratio on the retention of molecular iodine, two other Ag/Y sorbents were obtained by Incipient Wetness Impregnation (IWI). For comparison purposes, the silver loading in the impregnated zeolites was targeted to be also 23 wt%, which is similar to the mass percentage of the 3 times exchanged-silver zeolite (22.8Ag/Y 2.5). Two different faujasite Y zeolites were used: (i) the same NH₄Y zeolite as the one used for ion-exchange (Si/Al = 2.5, V_{porous} = 980 μL/g) and another HY zeolite with a much lower amount of exchange sites (Si/Al = 40, V_{porous} = 1080 μL/g). Once the pores saturated with the required amount of AgNO₃ solution, the samples were dried at 80°C overnight and further calcined at 500°C (procedure similar to ion-exchanged zeolites).

A “benchmark” Ag/13X zeolite (Si/Al=1.2, 382280, Ag₈₄Na₂[(AlO₂)₈₆(SiO₂)₁₀₆].xH₂O) with 35 wt% silver was also purchased from Sigma-Aldrich for comparison purposes. This zeolite was denoted thereafter 35Ag/13X_{comm} (1.2).

2.2. Physicochemical characterizations

Elemental ICP analyses (Ag, Na, Al and Si) were performed at the Service Central d’Analyses of the CNRS and at the Service d’Analyses des Roches et des Minéraux (France).

Powder X-ray diffraction (PXRD) measurements before and after test were carried out using a *Rigaku-Miniflex II* (Japan) with the CuKα radiation (λ= 0.15418 nm). PXRD patterns were recorded between 5 and 70° (2θ) using increments of 0.02° and a counting time of 2 s.

Porosimetric properties were determined from N₂ adsorption isotherms recorded at -196°C on an automated *Autosorb IQ* sorptiometer supplied by Quantachrome. Prior to each adsorption measurement, samples were outgassed *in situ* in vacuum at 80°C for 1h and then at 350 °C for 6h

to remove most of adsorbed impurities. Specific surface areas (S_{BET}) were determined using the BET equation ($0.05 < P/P_0 < 0.35$).

DRS UV-Vis spectra were collected on a *Varian Cary 4000 UV-Vis* spectrometer equipped with a double monochromator and *DR4900* integrating sphere. Spectra were registered between 200 and 800 nm, with a resolution of 2 nm and a scan rate of 600 nm/min. Reflectance spectra were plotted in pseudo-absorbance mode, after correction with a Spectralon standard (taken as reference).

2.3. I₂ adsorption – liquid-phase experiments

A screening of zeolitic materials towards I₂ retention was first carried out in liquid medium. Cyclohexane was used as solvent due to its ability to solubilize large amounts of iodine crystals (2.719 g I₂ for 100 g of C₆H₁₂ at 25°C) while maintaining I₂ in its molecular state (pink solution with two absorption maxima at 223 and 523 nm). For most of the tests (unless otherwise mentioned), 75 mg of sorbent was contacted at room temperature and in the dark with 50 mL of a 400 ppm solution made from I₂ pellets (*Alfa Aesar*, 99.5%). Determination of adsorbed amounts at equilibrium (duration 24 or 48 h, depending on the experiments) was done using UV-visible spectrophotometry from absorbance measurements at 523 nm using Beer's Law:

$$A_{523} = 3.5362 \times [I_2], R^2 = 0.9992 \quad \text{Eq. (1)}$$

2.4. I₂ vapor adsorption in dynamic conditions (breakthrough curves)

Retention properties of some selected zeolitic sorbents towards I₂ were further studied from gas-phase dynamic sorption tests at 100°C using a completely original experimental setup (Fig. 1), which could be divided in three parts:

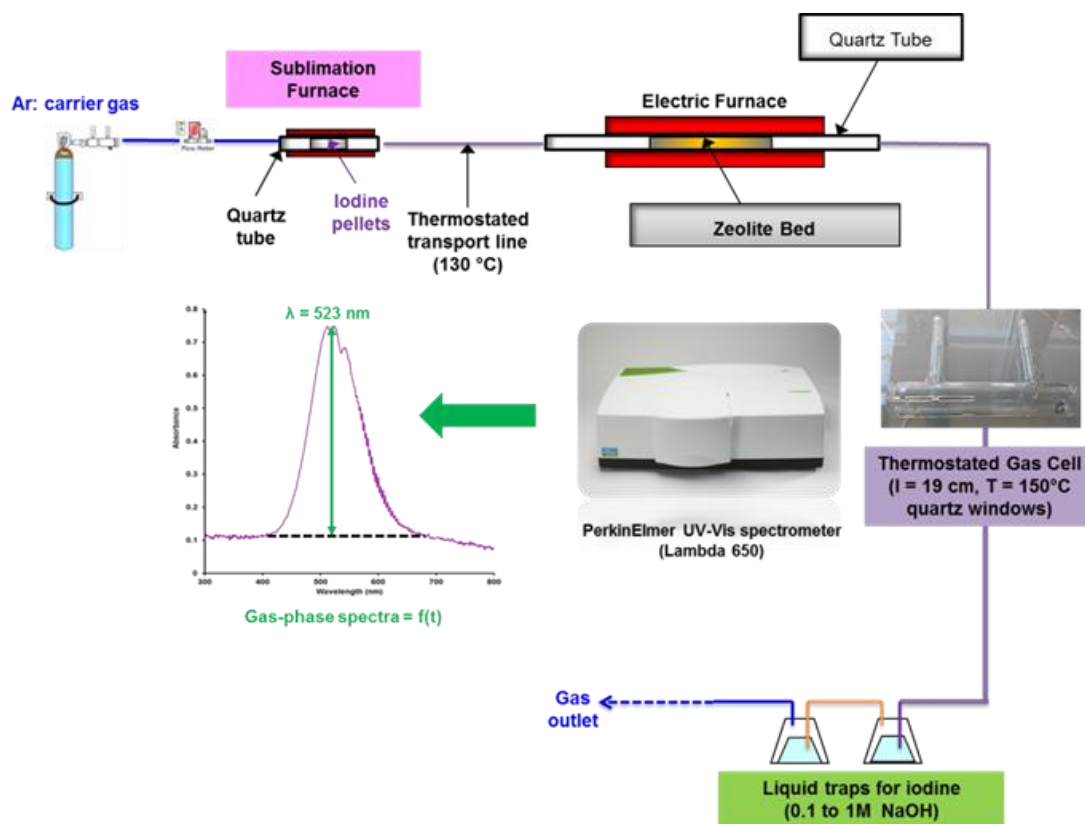


Figure 1: Experimental setup dedicated to I_2 adsorption by zeolitic sorbents under gas-phase dynamic conditions.

The first part is dedicated to the generation of a constant and reproducible concentration of I_2 from the controlled sublimation of iodine pellets. In that respect, a known mass of I_2 crystals was mixed with glass beads (in order to limit crystals coalescence²³) in a boat crucible, itself placed in a home-made sublimation furnace, whose working temperature can be finely regulated. According to the tendency of gas-phase iodine to condensate as solid deposits into cold points of the experimental setup, extreme care was taken to adequately heat all transfer lines (to $100\text{ }^\circ\text{C}$ for the part before the detection cell and $130\text{ }^\circ\text{C}$ after using 5 different *Eurotherm 2116* temperature controllers and K-type thermocouples, Fig. 1), except the part before the sublimation furnace, which was pre-heated to $50\text{ }^\circ\text{C}$).

With the aim to reach the adsorption capacity of the sorbents over a reasonable period of time (a few hours at the most), preliminary experiments were achieved in order to optimize the I₂ concentration. Under dynamic conditions, it is important to mention that the concentration (or partial pressure) of iodine vapor does not solely rely on the sublimation temperature (as for static conditions²⁴), but also depends on other parameters, such as the flow rate of the diluting gas (Ar in our case) and the iodine initial mass. In each experiment, the temperature of the sublimation furnace was set to 50 °C, the Ar (Air Liquide, 99.99%) flow to 100 mL/min (using a *EL-FLOW* mass-flow controller from *Bronkhorst*) and the mass of iodine pellets (*Alfa Aesar*, 99.9 %) to 4 g. As determined from blank tests in absence of sorbents, this allowed us to obtain a stable concentration (for a sufficient period of a few hours) of I₂ diluted in Ar equal to 1250 ppm, according to the gas-phase UV-Vis detection method used ($\epsilon \approx 730 \text{ L}\cdot\text{mol}^{-1}$ at 523 nm²⁵, *see next for details*). Because the iodine concentration determined by spectrophotometry depends on the accuracy of the extinction coefficient, it was compared with the values measured from other methods, including the continuous weighing of iodine-containing crucibles or total iodine analysis by ICP-MS in NaOH liquid traps over a fixed period of time. A reasonable agreement was found between both methods ($\pm 15\%$).²⁶ We chose to use the spectrophotometric method, because it allows the continuous monitoring of the I₂ concentration in the gaseous phase with good accuracy and enough sensitivity.

In the second part of the system (Fig. 1), the gaseous flow (loaded or not with iodine) feeds a home-made fixed-bed reactor containing the sorbent (200 mg, pelletized and sieved between 200 and 630 μm , bed length $\approx 2 \text{ cm}$) placed itself in a glass tube (internal diameter 4 mm) and maintained between two pieces of quartz wool. Before each I₂ retention test, the sorbent is *in situ* pre-treated to 150°C (5°C/min, 2 hours) under Ar (60 mL/min) in order to remove most of the

adsorbed moisture. Then, the sorbent is cooled down under Ar up to the adsorption temperature (100°C). Once the sorbent is saturated with iodine, an evacuation step under Ar (200 mL/min) is done (still at 100°C) in order to eliminate all the weakly adsorbed iodine species. Typical signals obtained through this procedure are shown on Fig. 2.

Finally, the last part of the system is the UV-visible detection/quantification setup. It consists in a dual-beam *Perkin Elmer* Lambda 650 UV-visible spectrophotometer, whose sample compartment is sufficiently large to welcome a gas cell of pathlength 19 cm ($V = 0.072$ L) fitted with two quartz windows and heated to 150°C. NaOH liquid traps were added at the outlet of the gas cell to remove gas-phase iodine before it escapes into the environment. On-line measurements were carried out using the WinLab software by acquisition of UV-visible spectra (resolution 1 nm, response time 0.16 s, slit height 2 nm, Ar as spectral reference) of gaseous iodine between 300 and 800 nm every 3 min during I_2 adsorption/desorption phases. Continuous monitoring of I_2 concentrations was done from repeated absorbance measurements at $\lambda_{\max} = 523$ nm, which allows us to obtain good quality breakthrough curves and desorption data. Under these conditions, the detection limit was about 10 ppm. Adsorption capacities (Q_{sat}) at saturation were calculated from integration of I_2 breakthrough curves (Fig. 2) through the following equation (Eq. (2)):

$$Q_{\text{sat}} = \frac{D \times \int_{t_i}^{t_f} ([I_2]_{\text{in}} - [I_2]_{\text{out}}) dt}{m} \quad \text{Eq. (2)}$$

Where:

- D is the total flow rate ($\text{mL} \cdot \text{min}^{-1}$);
- m is the weight of material introduced into the reactor (g);
- $[I_2]_{\text{in}}$: the gas inlet concentration (ppm_v);
- $[I_2]_{\text{out}}$: the gas outlet concentration (ppm_v);

- t_i : the time corresponding to Ar substitution by I_2 (0 min) ;
- And t_f (min) is the time of bed saturation ($C/C_0 = 1$).

Subtraction of the value obtained from a blank experiment was also done for better accuracy. Adsorption capacities at breakthrough ($Q_{\text{breakthrough}}$) were also quantified using Eq.2, using $t_{5\%}$ (corresponding to $C/C_0 = 0.05$) instead of t_f .

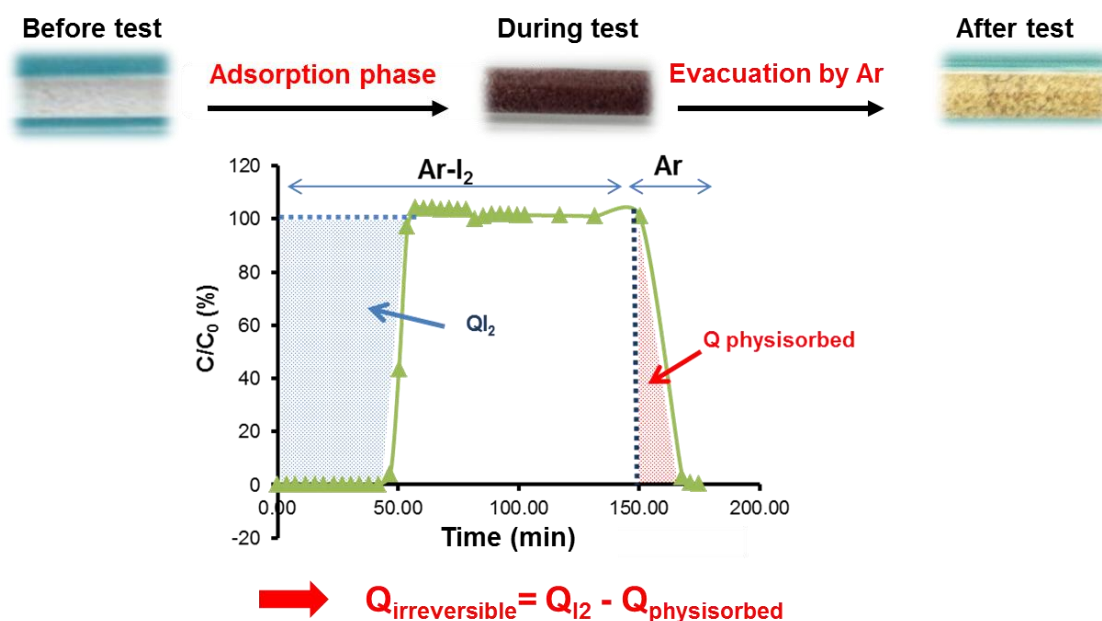


Figure 2: Typical breakthrough and desorption profiles observed during gas-phase I_2 sorption experiments and associated color changes in zeolite bed.

2.5. Description of EPICUR irradiation studies

The EPICUR facility was used in order to check the stability of iodine trapping by silver zeolite upon irradiation. The experimental set-up used to study the effect of irradiation consists of a panoramic irradiator and an electro-polished stainless steel irradiation vessel (containing the I_2 -loaded zeolite, Fig. S1 in ESI) connected through stainless-steel tubes to an iodine filtration system, called *Maypack* (Fig. 3). In this experimental loop, the irradiation vessel receiving the

dose rate from the irradiator simulates the reactor containment. The panoramic irradiator containing ^{60}Co sources is designed to deliver an average dose rate of several $\text{kGy}\cdot\text{h}^{-1}$ in order to mimic the effect of radiations delivered by fission products in the reactor containment during the **accident**.

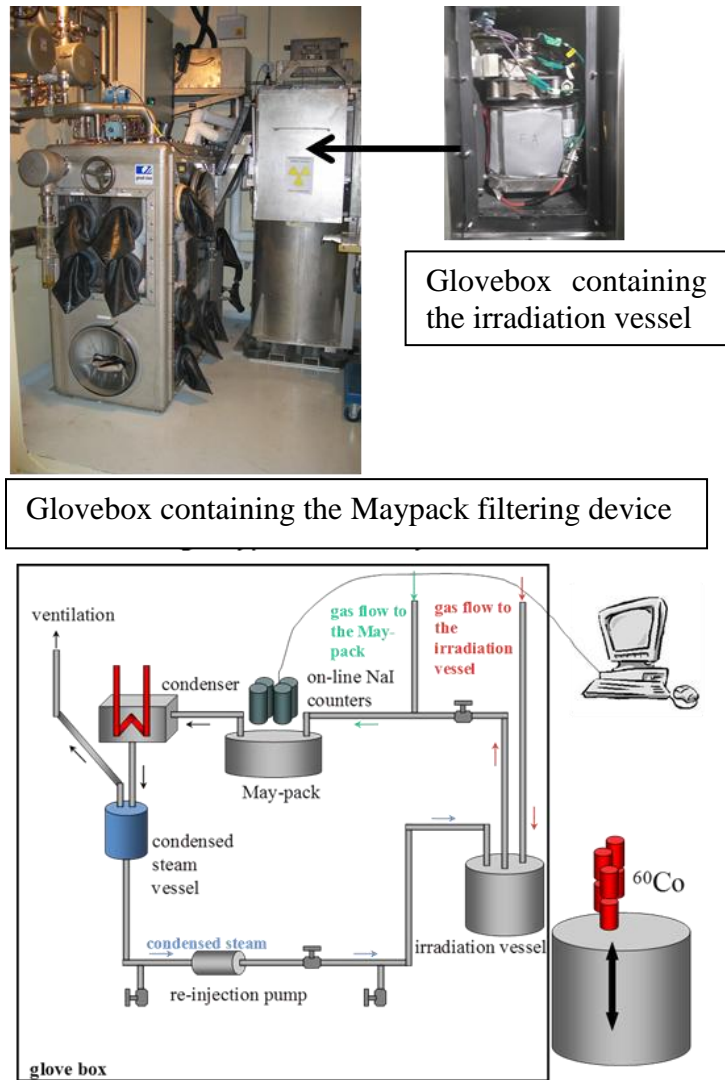
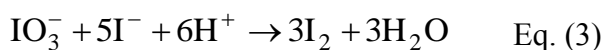


Figure 3: Scheme of the EPICUR facility.

Loading of radioiodine into zeolite filter. The studied silver zeolite is the commercial sorbent labelled 35Ag/13X_{comm} (grain size 841 µm/20 mesh). 8.7 g of zeolite were loaded in each of 3 identical holders (named Z1, Z2 and Z3) of diameter 30.6 mm and thickness 23 mm (Fig. 4). A final holder filled with activated charcoal (labelled CADT4 on Fig. 4) was added in order to prevent any loss of radioiodine during the loading phase. The filter body is subsequently closed and connected to the iodine generator.

Molecular iodine (labelled with ¹³¹I) was produced from the Dushman reaction²⁷ at 50°C by injection of sulfuric acid (final pH = 3) to an initially basic solution (pH = 12) containing Na¹³¹I and sodium iodate.



Molecular iodine is transported by a N₂ flow through the zeolite holders at a velocity of 59 cm/s (flow rate 35 L/min).

The radioiodine gas loaded into the different zeolite holders is then measured by gamma spectrometry (using NaI(Tl) probes and Interwinner – Itech software). Accurate measurements of gaseous radioiodine activity in the silver zeolite holders were achieved thanks to internal calibrations (see iodine loading in mg/g in Z1, Z2, Z3 holders in Table 1).

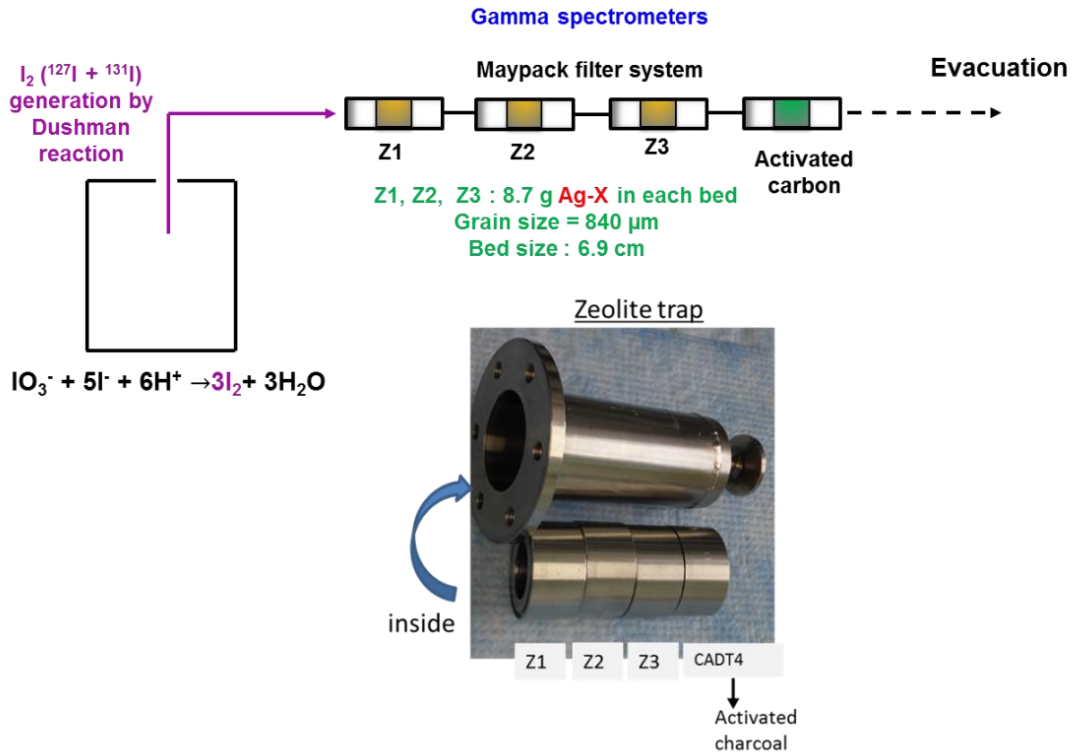


Figure 4: Experimental setup describing the loading of 3 consecutive zeolite beds (35Ag/13X_{comm} (1.2), Z1, Z2, Z3) by molecular iodine and isotopic labelling by ¹³¹I before EPICUR tests.

Description of irradiation tests. The 3 zeolite holders loaded with iodine (ZEO1 test in Table 1) were installed in a support itself connected to the bottom of the temperature-controlled irradiation vessel. During the pre-irradiation phase (Table 1), the vessel is heated to the targeted temperature (120°C) and pressure (~3.5 bar) under flowing wet air (relative humidity (R.H) of 60%, velocity through zeolite holders 0.4 cm/s) during 1h. During the irradiation phase (30 h, dose rate of 2.9 kGy/h), the temperature of the vessel is maintained at 120°C and the absolute pressure at 3.5 bar. The air flow is 17 g/h and the steam flow is 5.5 g/h (60% R.H.) through the irradiation vessel. After the irradiation phase, the irradiation vessel is swept with wet air during 3h then with dry air during 1h.

During the irradiation test, re-volatilization of the trapped iodine could occur. If so, the volatile species produced in the irradiation vessel are transferred to different filters (*Maypack*) designed to trap selectively iodine aerosols (Quartz Fiber filter (QF)), inorganic iodine (Knit-mesh filter (KM) with silver clad copper) and then organic iodides RI (KI impregnated charcoal filter (CF)). Thanks to the use of radioactive iodine, continuous γ -measurements could be performed on the *Maypack* filter stages (NaI counters are placed above each filtration stage of the *Maypack* device) in order to on-line quantify the amount of the different species volatilized then trapped on the selective filters. At the end of the irradiation phase, the *Maypack* iodine filtration system was recovered. The different filters, the zeolite holders and the washing solutions of the irradiation vessel were also γ -counted after the test in order to compare these post-test measurements with on-line measurements (and to calculate the overall iodine mass balance). Gamma measurement uncertainties are estimated to be around 10%.

Two different tests were conducted in order to also assess the effect of an irradiation pre-treatment on the silver zeolite (before it is loaded with radioiodine). Conditions used for the tests performed without pre-treatment (ZEO1) and on the pre-irradiated zeolite (ZEO2) are compared in Table 1. For ZEO2, the three zeolite holders were pre-irradiated in the IRMA γ -irradiator facility at IRSN during 172 h at an average dose rate of 12.9 kGy/h (total dose 2.2 MGy).

Parameter	ZEO1	ZEO2
Pre-irradiation of the zeolite before I ₂ adsorption	No	2.2 MGy
Temperature (°C)	120	
Pressure (bar)	3.5	
Gas composition	Moist air (R.H of 60%)	
Total flow rate	20	
Velocity (cm/s)	1	
Irradiation duration (h)	30	
Average dose rate (kGy/h)		
Z1	1.6 to 2.0	
Z2	2.0 to 2.6	
Z3	2.6 to 4.3	
Iodine loading (mg/g of zeolite)		
Z1	8.2	9.3
Z2	3.8	3.1
Z3	0.5	0.4

Table 1: Experimental matrix for irradiation tests.

3. RESULTS AND DISCUSSION

3.1. Characterization of silver zeolites

Characterization of silver-exchanged zeolites by XRD, DRS-UV-Vis, elemental analyses and N₂ porosimetry at 77K, was already reported in our previous study¹³ and will therefore not be described in detail here. Briefly, it was found that Ag-exchanged zeolites have silver contents

between 3.4 and 23.4 wt% (except the commercial 35Ag/13X_{comm} (1.2) zeolite, which has 35 wt% silver), depending on the parent structure and the Si/Al ratio (Table 2). As expected, highest silver contents were achieved with faujasite-type (FAU) zeolites (Ag/Y and Ag/X owing to their high concentrations of exchange sites) and after repeated ion exchanges. For all exchanged-zeolites, the determination of Ag/Al ratio below 1 from elemental analyses, corresponding to theoretical maximum exchange degrees less than 100 %, ensures that extensive silver agglomeration did not take place (as confirmed from XRD data, which did not indicate the presence of Ag-containing phases). Nevertheless, it was found from Diffuse Reflectance UV-visible Spectroscopy that all silver-exchanged zeolites contain, besides the presence of Ag⁺ cations on exchange sites, Ag_n^{δ+} and/or Ag_m[°] clusters in different proportions within their porous systems. In the literature, the formation of clustered species is well known and was reported to be rather typical of silver zeolites. It was explained from the existence of silver auto-reduction processes occurring namely during thermal activation.^{28,29}

It is interesting to compare the properties of Ag/Y sorbents obtained from impregnation (corresponding to labels IWI in Table 2) with those of the ion-exchanged Ag/Y zeolite (22.8Ag/Y (2.5)) having identical silver content (23 wt%). The impregnated 23Ag/NH₄-Y (2.5)_IWI sorbent is characterized by a Si/Al ratio identical (2.5) to the one of ion-exchanged Ag/Y and exhibits comparable porosimetric and chemical properties. All the silver in the 23Ag/NH₄-Y (2.5)_IWI sorbent was found also to be rather finely dispersed in the pores, as revealed from XRD and DRS-UV-Vis data (Fig. S2 (A1)&(A2) in ESI). This could be reasonably understood considering that ion exchange reactions probably took place during impregnation due to the high concentration of exchange sites present in the pores. By contrast, the 23Ag/H-Y (40)_IWI sorbent has comparatively very few exchange sites due to its high Si/Al

ratio (40, corresponding to Ag/Al = 6.4). Hence, most of the silver was found to be agglomerated as metallic zerovalent nanoparticles on the external surface, showing a behavior close to $\text{Ag}^\circ/\text{SiO}_2$ supported catalysts (Fig. S2 (A1&A2) in ESI). Accordingly, the surface specific area of this sample is decreased by *ca* 25 %, as compared with the other Ag/Y zeolites, this being presumably due to the occlusion of some micropores by silver nanoparticles.

3.2. I_2 sorption properties in liquid phase (cyclohexane, $T = 25^\circ\text{C}$)

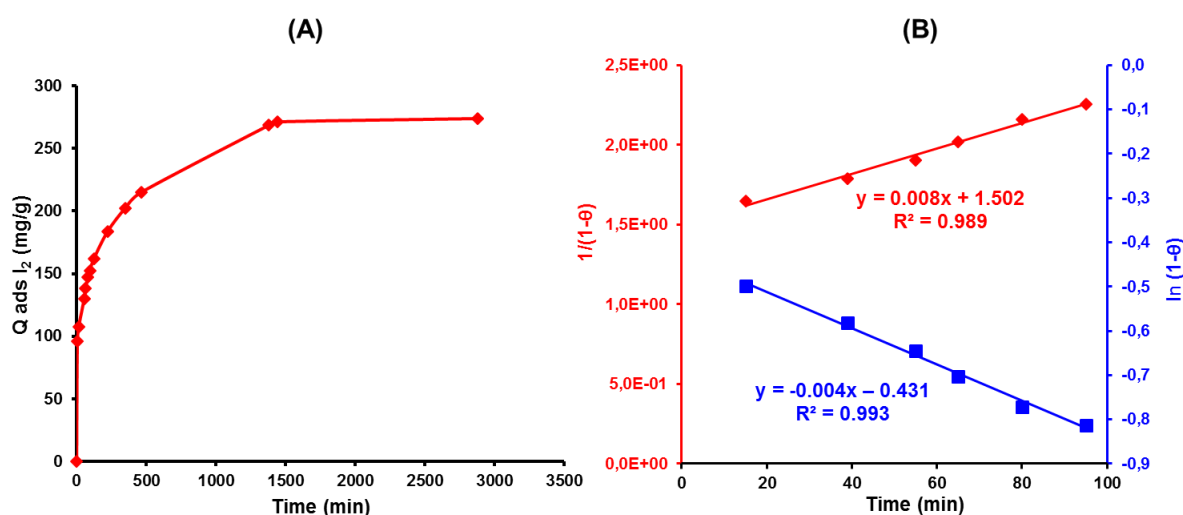


Figure 5: (A) Kinetics of I_2 uptake by 35Ag/13X_{comm} (1.2) ; (B) Modeling of adsorption kinetics using an order of 1 (blue) or 2 (red). $T = 25^\circ\text{C}$, $[I_2]_0 = 800$ ppm, $V = 200$ mL, $m = 300$ mg.

I₂ adsorption kinetics. The I_2 uptake versus time is plotted on Fig. 5 (A) for the commercial 35Ag/13X_{comm} (1.2) sorbent for an initial iodine concentration of 800 ppm in cyclohexane. It is observed that the adsorption equilibrium is reached after approximately 24 hours (corresponding to a total uptake Q_{max} of 270 mg/g), as shown by the presence of a plateau in Fig. 5 (A).

Zeolite	S_{BET} (m²/g)	Silver speciation	Q I₂ (mg/g)	I/Ag
H/Y (2.5)	845	H⁺	10	-
9.1Ag/Y (2.5)	744	Ag⁺, Ag_n^{δ+}, Ag_m^o	123	1.15
16.8Ag/Y (2.5)	541	Ag⁺, Ag_n^{δ+}, Ag_m^o	207	1.05
22.8Ag/Y (2.5)	704	Ag⁺, Ag_n^{δ+}, Ag_m^o	269	1.00
22.8Ag/Y (2.5)_irradiated	682	Ag⁺, Ag_n^{δ+}, Ag_m^o	265	0.99
23Ag/NH₄-Y (2.5)_IWI*	704	Ag⁺, Ag_n^{δ+}, Ag_m^o, Ag^o (traces)	260	0.96
23Ag/H-Y (40)_IWI*	493	Ag^o nanoparticles (9.5 nm)	255	0.94
7.3Ag/13X (1.2)	578	Ag⁺, Ag_n^{δ+}	116	1.34
23.4Ag/13X (1.2)	472	Ag⁺, Ag_n^{δ+}	255	0.93
35Ag/13X_{comm} (1.2)	369	Ag⁺, Ag_n^{δ+}, Ag_m^o	280	0.68
5.9Ag/MOR (10)	521	Ag⁺, Ag_n^{δ+}	62	0.89
7.3Ag/MOR (10)	486	Ag⁺, Ag_n^{δ+}	77	0.91
3.4Ag/BETA (10.1)	487	Ag⁺, Ag_n^{δ+}	58	1.44
5Ag/MFI (11.5)	359	Ag⁺, Ag_n^{δ+} (traces)	63	1.09
H/FER (10.4)	383	H⁺	9	-
4.2Ag/FER (10.4)	357	Ag⁺, Ag_n^{δ+}	64	1.28

Table 2: Characterization data of silver zeolites and I₂ adsorption capacities obtained from liquid-phase experiments at T = 25°C.

After-test characterization of the sorbent by XRD revealed the presence of AgI nanocrystallites (β polymorph, Fig. S3 in ESI) of mean size about 23.5 nm (as computed from Debye-Scherrer

equation). According to our previous study¹⁰, it seems that molecular (AgI)_n species are produced first inside the pores and then further coalesce to give larger AgI precipitates outside of the pores, consistently with the yellowish color of silver zeolites after adsorption tests.

For these types of adsorption phenomena involving dissociative chemisorption processes, it could be convenient to use the fraction of remaining vacant sites (1-θ, with θ being the surface coverage defined as Q/Q_{max}) instead of simply the adsorbed amount (such as Q_{adsI2} in Fig. 5 (A)) in order to model the adsorption kinetics. Our attempts to model the filling of free adsorption sites with orders 1 or 2 were found to be both satisfying (R² ≈ 0.99), indicating that the adsorption of molecular iodine probably involves complex kinetics, owing to the existence of successive or competing reactions.

In the first minutes (Fig. 5 (A)), the concentration of free adsorption sites is high and the I₂ uptake is very rapid. AgI formation could be first schematically represented by the equation:



This global equation can be considered as resulting of the following elemental processes, one probably occurring at a much higher rate than the other, resulting in non-differentiated 1st or 2nd order kinetics:



In the course of the formation and growth of AgI species, some pores are getting progressively occluded and diffusional limitations arise for the transport of novel I₂ molecules towards the remaining free adsorption sites. As a result, the uptake rate slows down (part of the curve after 100 min in Fig. 5 (A)). Moreover, non-dissociative chemisorption and physisorption processes could also be considered to contribute to the total uptake resulting in complex kinetic behavior.

I₂ adsorption isotherm. Determination of the adsorption isotherm (Fig. 6 (A)) was also done for the 35Ag/13X_{comm} (1.2) sorbent under the following conditions ($[I_2]_0$ in the range 200-2500 ppm, $V = 50$ mL, $m = 75$ mg, $T = 25^\circ\text{C}$, $t_{\text{eq}} = 48$ h). For this sorbent with a high amount of silver (35 wt%), iodine is totally retained for initial $[I_2]_0$ concentrations inferior to 400 ppm. The rapid increase of the adsorbed amount in the low concentrations domain, followed immediately by a plateau (denoting surface saturation), is indicative of strong adsorption (chemisorption). The shape of the isotherm measured for silver zeolite is markedly different to the isotherms obtained with MOFs.³⁰ For the latter sorbents, I_2 adsorption mainly involves Van der Waals (weak) electrostatic interactions with the surface. Hence, the increase in adsorbed amount is much more progressive, surface saturation being reached only at high concentrations (> 2000 ppm). For silver zeolite, the main process involved in I_2 uptake is the chemical reaction between silver sites and molecular iodine, forming AgI precipitates. As shown earlier,¹³ this process is more dependent on the availability of silver surface sites than on the initial I_2 concentration (as expected for physisorption-type adsorption isotherms).

Common models used to describe chemisorption are Langmuir, dissociative Langmuir and Temkin isotherms (see ESI for a description of these models (S4 (A))). In our case, all these types of isotherms gave a good fit with our experimental data (Q_{max} values in the range 270-290 mg/g, S4 (B)). The total iodine uptake in the low concentrations domain was better fitted with dissociative Langmuir or Temkin models while the classical Langmuir model better described the behavior at higher concentrations (near the plateau).

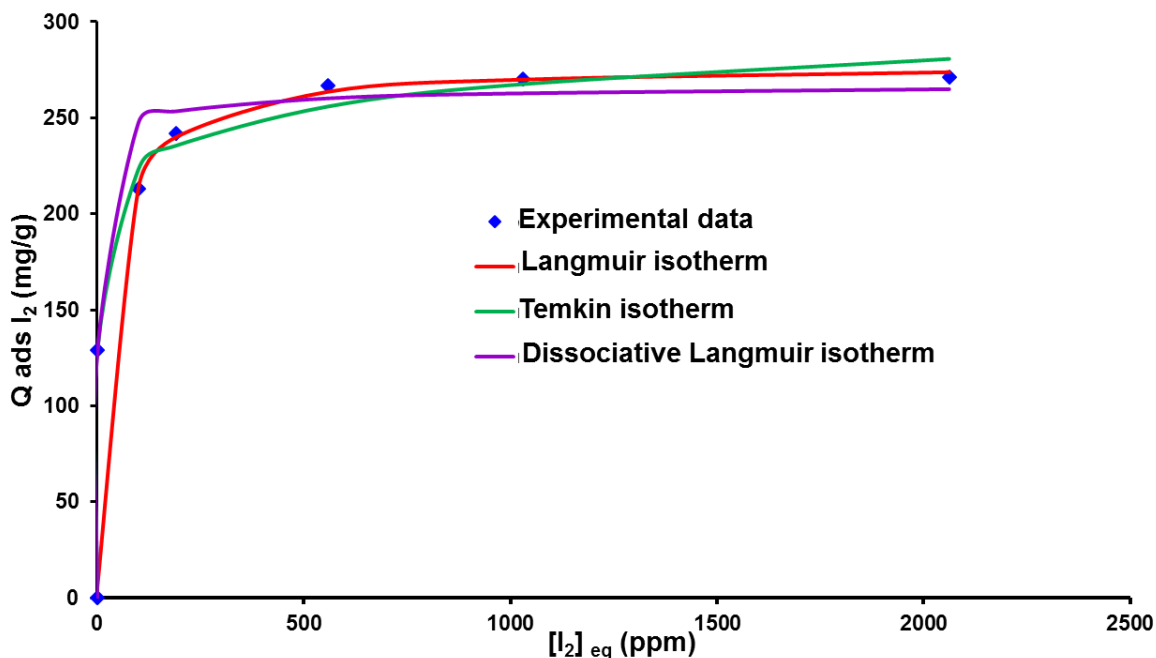


Figure 6: Experimental I₂ adsorption isotherm at T = 25°C for 35Ag/13X_{comm} (1.2) zeolite and results of modeling using using Langmuir, Temkin and dissociative Langmuir models.

Comparison of silver zeolite sorbents. In this part, we aimed to investigate the effects of some zeolitic parameters, such as the silver content, the parent zeolitic structure or the Si/Al ratio (for faujasite-type zeolites X and Y) on iodine adsorption.

I₂ adsorption capacities at saturation corresponding to the sorbents listed in Table 2 are plotted in function of the silver content on Fig. 7. For the different series of silver zeolites, it can be seen that a quasi-linear relationship exists between the silver content and the I₂ adsorption capacities. Such type of relationship was also obtained in our previous study related to the adsorption of CH₃I under gas-phase dynamic conditions (T = 100°C).¹³ This indicates that the sorbents efficient for CH₃I adsorption are also the best for molecular iodine adsorption.

In the present study, zeolites in protonated form (H/FER (10.4) and H/Y (2.5)) showed almost no iodine adsorption (Q_{sat} < 10 mg/g), confirming again that silver sites are mandatory for iodine

retention. By contrast with the silver content, the textural properties of the parent zeolites, such as the pore size, the specific surface area or the type of pore connectivity, have only a very limited effect. Apparently, no restriction due to the pore size is observed, except perhaps for the small-pore silver ferrierite zeolite (4.2Ag/FER (10.4)). For this sorbent, after-test characterizations confirmed the presence of two types of adsorbed species: AgI precipitates (characterized by an absorption edge at 412 nm in the UV-Vis spectrum and new peaks located at 39.30 and 46.64° (2 θ) in XRD pattern, see Fig. S5 (B) in ESI) and physisorbed iodine (as deduced from the pink color of the sample after test and the presence of a broad band around 510 nm in UV-Vis spectrum, see Fig. S5 (A) in ESI). For silver ferrierite, it seems that iodine physisorption could be promoted at the expense of AgI formation because of its small pore size (3.5 x 4.8 Å; 4.2 x 5.4 Å), rather comparable to the size of I-I chains (kinetic diameter 3.35 Å²⁰). Nevertheless, this sorbent does not show significant deviation to the linear relationship, even when compared with large-pore faujasites (Ag/X and Ag/Y) or mordenites (Fig. 7).

In general I/Ag ratio close to unity could be computed from the measured adsorption capacities. This indicates a total use of silver atoms for iodine adsorption, corresponding to the formation of AgI as the main adsorption product (as confirmed by after-test characterization). Hence, it appears that the affinity of I₂ towards silver is so strong that the thermodynamics of iodine adsorption are almost not affected by the initial state and location of silver within the different zeolitic frameworks. This is further confirmed by several facts. First, the formation of large AgI precipitates was observed for all silver zeolites after test by XRD, which indicates that silver is expelled from the pores in the course of the adsorption process, promoting the rapid sintering and coalescence of AgI entities. Second, it is interesting to compare the adsorption capacities (and related I/Ag values, Table 2) measured for Ag/Y impregnated zeolites with the

one obtained for the silver-exchanged Y zeolite with similar Ag content (23 wt%). The 23Ag/HY (40)_IWI sorbent, with almost no exchange sites and all the silver initially present as zerovalent nanoparticles on the external surface, has almost the same adsorption capacity (255 mg/g, I/Ag = 0.92) than the 23Ag/NH₄Y (2.5)_IWI and 23Ag/Y (2.5) sorbents, with most of the silver present as Ag cations or small clusters in their internal surface. Hence, this confirms that the initial oxidation state and dispersion of silver has almost no effect on the adsorption capacities measured at thermodynamic equilibrium ($t_{eq} = 24$ h).

Nevertheless, some sorbents showed some deviations towards the general behavior (Table 2, Fig. 7), which could be at least partly explained. The I/Ag ratio of 0.68 obtained for the commercial 35Ag/13X_{comm} (1.2) sorbent stands probably from its very high content in silver. Such high concentration of silver probably induced the occlusion of some micropores as AgI precipitated entities formed, thereby hindering the accessibility of new iodine molecules towards silver atoms located at the centre of zeolite crystallites. On the other hand, the I/Ag ratio of 1.34 measured for the 7.3Ag/X (1.2) zeolite is probably overestimated due to the contribution of sodium sites (5.86 wt% in this sample) as secondary (weak) sites for iodine adsorption, forming NaI entities in addition to AgI precipitates. At low silver contents and when pore size restrictions could be present (case of 3.4Ag/Beta and 4.2Ag/FER), it is possible that the contribution of physisorption processes also led to an overestimation of I/Ag ratio (Table 2).

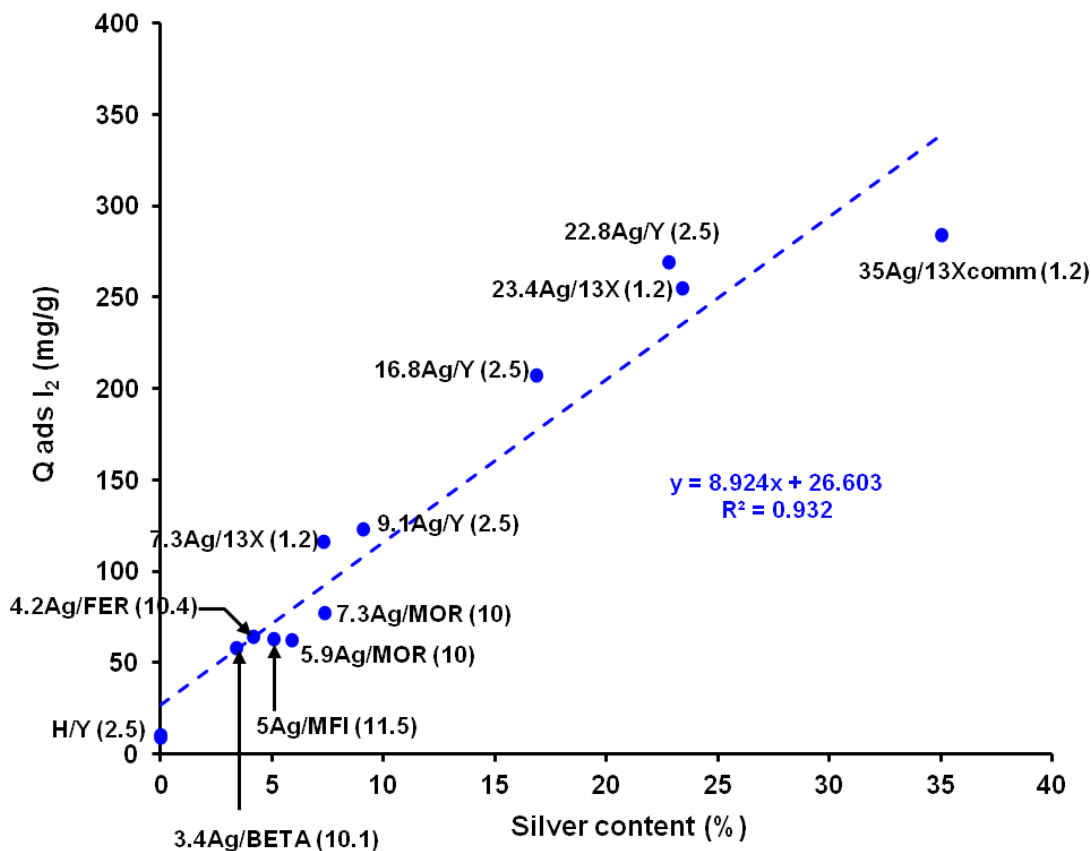


Figure 7: I₂ adsorption capacities ($[I_2]_0 = 400$ ppm, $m = 75$ mg, $V = 50$ mL, $T = 25^\circ\text{C}$, $t_{\text{eq}} = 24$ h) in function of silver content for the exchanged-silver zeolites.

3.3. Gas-phase dynamic I₂ sorption properties ($T = 100^\circ\text{C}$)

Sorbents having displayed the best adsorption performances in liquid medium at 25°C (exchanged or impregnated Ag/Y zeolites with *ca* 23 wt% silver and the commercial 35Ag/13X_{comm} (1.2) sorbent) were selected for gas-phase dynamic iodine sorption tests (fixed-bed experiments). The temperature of 100°C was chosen because it is representative of severe accidental conditions inside the nuclear containment building.⁶ I₂ breakthrough curves are shown on Fig. 8 and quantitative data extracted from these experiments are given in Table 3. Overall, the adsorption capacities measured under gas-phase dynamic conditions at 100°C (Table 3) were found to be slightly above those measured in liquid-phase experiments (Table 2). This may be

related to an effect of the adsorption temperature (the cleavage of the I-I bond required for the formation of AgI is promoted at 100°C) or to the absence of solvent during gas-phase tests (the intracrystalline diffusion of iodine is promoted for the gas while the solvent may occupy some adsorption sites or some space in the pores during liquid-phase experiments).

Iodine adsorption capacities. As observed on Fig. 8, the profiles measured obtained for the different silver faujasite zeolites have a classical S-shape with a steep increase of the concentration of gaseous I₂ after breakthrough. In agreement with the low L_T/L values (0.2-0.3) in Table 3, this indicates the absence of significant resistance as iodine diffuses from the external surface towards the bulk of zeolite crystallites. Consequently, the useful working capacities of these zeolites (corresponding to Q_{breakthrough} values in Table 3) are close to the adsorption capacities measured at saturation (Q_{sat} in Table 3). The highest adsorption capacities (Q_{sat} = 380-400 mg/g and Q_{breakthrough} = 325-330 mg/g) were measured for the 3 times ion-exchanged Ag/Y zeolite (22.8Ag/Y (2.5)) and the commercial Ag/X sorbent. The commercial sorbent having about half more silver than for the Ag/Y exchanged zeolite (35 wt% against 23 wt%), this probably confirms that the accessibility to some silver sites is hindered (presumably due to pore occlusion following the formation of AgI) when the silver content exceeds a certain level (about 25 wt% for faujasite zeolites).

Second, it is also worth noting that an irradiation pre-treatment (⁶⁰Co source, total dose 1.14 MGy) performed on the 3 times exchanged Ag/Y zeolite did not change its retention properties. This is not surprising considering that neither the silver speciation nor the structural or textural characteristics of this material were found to change after pre-irradiation (as deduced from the similarities existing between XRD patterns and DR-UV-Vis spectra before/after irradiation (Fig. S2 (A3&A4) in ESI).

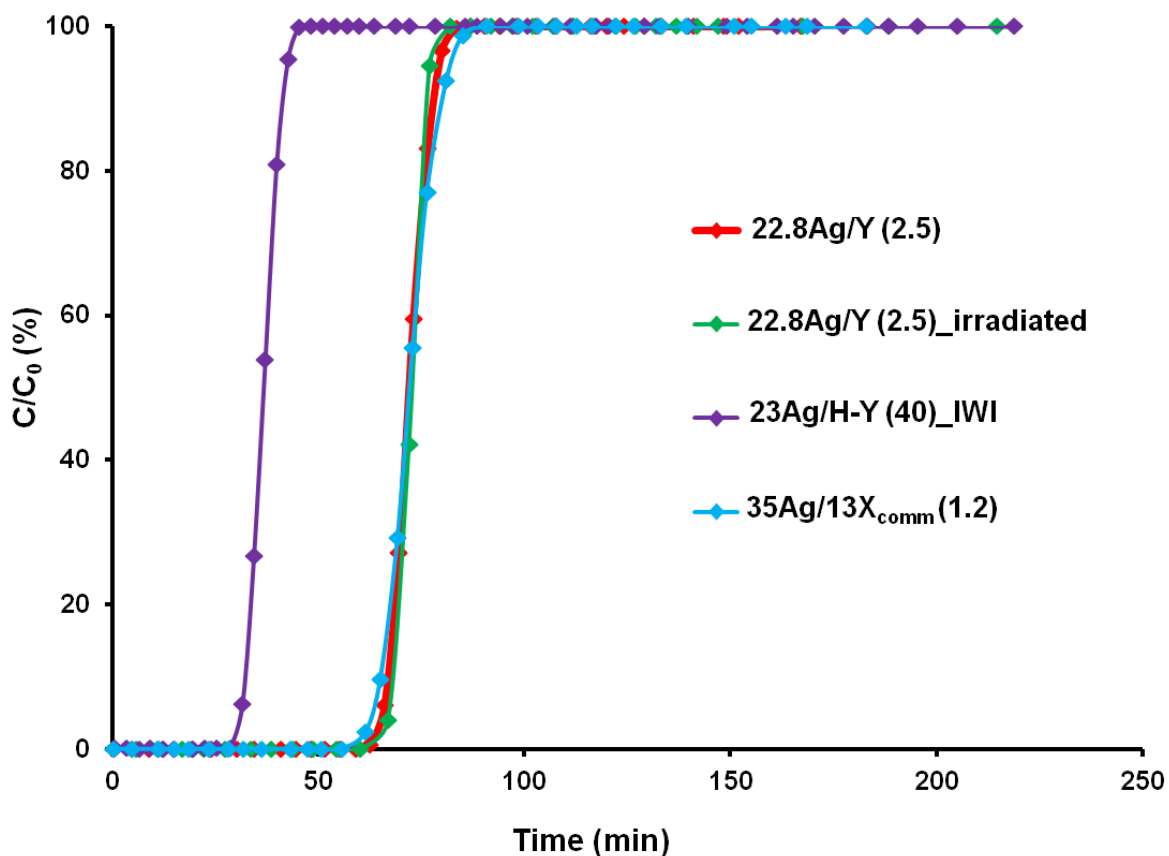


Figure 8: I₂ breakthrough profiles measured for a selection of silver zeolites (T = 100°C, [I₂]₀ = 1250 ppm).

The effect of the preparation method (ion exchange vs impregnation) can be also assessed by comparing the data obtained for 22.8Ag/Y and 23Ag/HY (40)_IWI, respectively (Table 3 and Fig. 8). In stark contrast with liquid-phase experiments, the adsorption capacities measured for the impregnated 23Ag/HY (40)_IWI material are this time divided by a factor higher than 2. We think that these differences in behavior have for origin the conditions employed for liquid and gas-phase experiments in relation with the initial state of silver in these two sorbents. For the impregnated 23Ag/HY (40)_IWI zeolite, the adsorbed iodine atoms have to diffuse from the surface to the bulk of Ag⁰ nanoparticles (mean size 9.5 nm, Table 2) to form an AgI phase.

Hence, such solid state diffusion process should be rather slow (kinetically limited even if promoted from a thermodynamic viewpoint). For the tests carried out in cyclohexane solvent at 25°C under static conditions, the equilibrium time is long (24 hours) and the formation of AgI precipitates from bulk Ag⁰ particles could be promoted, in contrast with dynamic gas-phase tests. In that respect, the size of AgI crystallites is noteworthy higher (Table 3) for the Ag-exchanged zeolite, presumably because the coalescence of AgI entities is made easier by the high initial dispersion of silver (no solid-state diffusion involved).

Zeolite	Q_{sat} (mg/g)	Q_{breakthrough} (mg/g)	t_{5%} (min)	L_T/L*	D AgI (nm)**
35Ag/13X_{comm} (1.2)	400	330	63	0.31	/
22.8Ag/Y (2.5)	380	325	65	0.25	46.2
22.8Ag/Y (2.5) irradiated	390	350	67	0.18	35.6
23Ag/Y (40)_IWI	184	137	30	0.37	22.4

* $\frac{L_T}{L} = \frac{t_f - t_{5\%}}{t_f}$, Where L_T is the length of the mass transfer zone, t_f (s) is the total equilibrium time (C/C₀ = 1), t_{5%} (s) is the time correspondent to C/C₀=0.05 and L is the bed length (cm).

** As estimated by XRD using Debye-Scherrer equation

Table 3: Adsorption performances of some selected zeolites under gas-phase dynamic conditions (T = 100°C, [I₂]₀ = 1250 ppm).

Iodine trapping stability.

Once the sorbents were getting progressively saturated by I₂, their color changed from white (for the exchanged zeolites) to deep purple (Fig. 2). Then, when surface saturation was reached, an evacuation step under Ar (200 mL/min) was added at 100°C in order to eliminate the weakly adsorbed species (Fig. 2). During this period, the intense purple disappeared and the samples turned yellow, due to the presence of AgI phase, as established in XRD patterns and DR-UV-Vis spectra recorded after-test (Fig. S6 (A&B) in ESI). The molecular form of adsorbed iodine, which could be removed by simple displacement of the adsorption equilibrium, will be referred thereafter as physisorbed species and was quantified by integration of the corresponding signals (Fig. 2, Table 4). Accordingly, the iodine fraction remaining trapped in the sorbents after the evacuation step will correspond to the irreversible adsorbed fraction (Table 4 and is estimated by establishing a matter balance with the total adsorption capacity (Q_{sat} values reported in Table 3):

$$Q_{\text{irreversible}} = Q_{\text{sat}} - Q_{\text{physisorbed}} \quad (\text{Eq. 7})$$

This irreversible fraction is mainly constituted by AgI precipitates (as deduced both from the yellowish color and from XRD and DRS-UV-Vis data after test, Fig. S6 (A&B) in ESI), but possibly also to a minor extent by other forms of adsorbed iodine, such as chemisorbed iodine or polymeric species.

Among the series of silver faujasite zeolites, the best performances in terms of trapping stability were obtained for ion-exchanged Ag/Y zeolite, with about 85% of irreversible trapping. The exposure of this material to an irradiation treatment before test (⁶⁰Co source, total dose 1.14 MGy) has no influence on its retention performances, which is in good agreement with liquid-phase experiments (Table 2) and characterization data (Fig. S2 (A3&A4) in ESI).

By contrast, reversible adsorption was more promoted for the impregnated Ag/Y zeolite (25%) and the commercial 35Ag/13X_{comm} (1.2) sorbent (40%). For the latter material, the high content

in silver (35 wt%) may limit the accessibility of iodine to some silver sites as some pores become plugged by the presence of AgI entities. Consequently, the amount of iodine trapped irreversibly is lower than for 22.8Ag/Y (2.5) (1.891 mmol/g against 2.545 mmol/g, Table 4). Such hypothesis is strengthened by the examination of I/Ag ratio in Table 4. By considering the I/Ag ratio corrected from the contribution of physisorption (last column in Table 4), a value of 0.58 is obtained for the 35Ag/13X_{comm} (1.2) sorbent. This clearly confirms that some silver atoms were not used for AgI formation. In opposition, the ion-exchanged 22.8Ag/Y (2.5) zeolite displayed much higher silver utilization (I/Ag = 1.19). On the other hand, the 23Ag/Y (40)_IWI impregnated zeolite is also characterized by a non-optimal use of silver (I/Ag = 0.51, Table 4). The formation of AgI from silver nanoparticles presenting a low surface/bulk ratio (in terms of silver distribution) will take place more easily on the most external layers due to some limitations imposed by solid-state diffusion. In other words, the most buried silver atoms in the particle core will not be accessible to iodine, resulting in a non-optimal I/Ag ratio.

Overall, the results obtained on iodine adsorption are consistent with our previous studies focused on CH₃I adsorption^{13,14}. Retention performances are mainly influenced by the silver content in the zeolite rather than by other zeolitic parameters, although the initial state of silver has also an important effect. High dispersion of silver as cations or embedded clusters in the pores is desirable for a better filtering efficiency. In that respect, the ion-exchanged Ag/Y sorbent with 23 wt% silver was found, among the series of investigated zeolites, to be the best in terms of adsorption capacities and trapping stability (by promoting AgI formation), exhibiting even superior properties than the commercial 35Ag/13X_{comm} sorbent with 35 wt% silver. For the latter, the aggregation of silver species in the pores may even lead to partial pore occlusion during iodine trapping, and such a high amount of silver is not desirable for economical reasons.

Sample	Physisorbed I ₂		Irreversible I ₂		I/Ag	
	(%)	Q _{physisorbed I} (mmol/g)	(%)	Q _{irreversible I} (mmol/g)	I/Ag global	I/Ag w/o physisorption
35Ag/13X_{comm} (1.2)	40	1.261	60	1.891	0.97	0.58
22.8Ag/Y (2.5)	15	0.449	85	2.545	1.40	1.19
22.8Ag/Y (2.5) irradiated	17	0.522	83	2.551	1.44	1.20
23Ag/Y (40)_IWI	25	0.362	75	1.087	0.68	0.51

Table 4: Reversible and irreversible adsorbed iodine fractions measured on some selected zeolites following breakthrough/desorption experiments.

3.4. Stability of iodine trapping under irradiation conditions

In this section, irradiation tests were performed onto the commercial 35Ag/13X_{comm} (1.2) sorbent (due to its availability in large amounts) with the aim to check that adsorbed iodine species could not be released from the zeolite upon simulated accidental conditions (T = 120°C, pressure 3.5 bar, wet air R.H. = 60%, 30 h of irradiation with a dose rate of 2.9 kGy/h). As reported in part 2.5., the silver zeolite was previously exposed to labelled iodine (¹³¹I₂) before the irradiation test. The zeolite holders were gamma-counted before irradiation and the initial activity measured was measured by NaI counters. Because the holders were placed in series during iodine exposure, the iodine loading logically decreases from holder Z1 up to holder Z3. It is worth noting that these loadings (all inferior to 10 mg/g, ZEO1 and ZEO2 tests in Table 1) only represent a small fraction (< 2-3 %) of the adsorption capacity at saturation of this sorbent (Q_{sat} = 400 mg/g in Table 3). This could be paralleled with the fact that under accidental

conditions (iodine concentration in the range 0.1-1 ppm⁶), the adsorption capacity of most sorbents for iodine will never be reached.

After the irradiation tests (ZEO1 and ZEO2, Table 5), the zeolite holders, the rinsing solutions of the experimental device (irradiation vessel, experimental loop and *Maypack*) and the *Maypack* filters were all gamma-counted in order to determine any decrease of activity in the zeolitic sorbent. Such a loss of activity could indicate the release of iodine *ad*-species in the gas-phase and therefore, an unstable trapping.

The results of post-test measurements are presented in Table 5, expressed in percentage of the initial activity loaded in the zeolite, *i.e.* before irradiation. The global release of iodine species corresponds to the difference between the activity of the solution after and before irradiation, it is expressed in percentage of the activity loaded in the zeolite before irradiation. On-line measurements are provided by four NaI counters placed above each of the four stages of filters of the *May-pack* device, allowing a continuous measurement of iodine release, including its speciation (see part 2.5.). However, it is worth noting that on-line gamma measurements are not as accurate as post-test measurements provided with gamma counting on each filter separately.

Tests	ZEO1	ZEO2
Initial activity in the zeolite (Bq)	$3.65 \times 10^5 \pm 3.6 \times 10^4$	$3.92 \times 10^5 \pm 3.9 \times 10^4$
Final activity in the zeolite after irradiation (%)	$3.68 \times 10^5 \pm 3.6 \times 10^4$	$3.79 \times 10^5 \pm 3.7 \times 10^4$
Activity on the quartz fiber filter (%)		
Activity on the knit-mesh filters (%)	Lower than Quantification limit (100 Bq)	Lower than Quantification limit (100 Bq)
Activity on the charcoal filters (%)		
Activity in the rinsing solutions (%)		
Iodine activity balance (%)	100	97.0 ± 3.0
Global releases (%)	0	lower than 3

Table 5: Post-test measurements.

Both for ZEO1 and ZEO2 tests, it can be seen from Table 5 that on-line and post-test measurements were all below the quantification limit (QL) (3000 and 100 Bq respectively, and some values were even at the detection limit (~20 Bq)). Activities measured on the zeolite before and after irradiation were similar, indicating the absence of iodine re-volatilization. The slight differences observed in the ZEO2 test are also not sufficiently significant to explain a possible iodine release. Despite the gas flow (0.4 cm/s), there is no iodine migration between zeolites holders. The zeolite irradiation tests have shown high stability of the material and/or iodine trapped, consistent with Evans's pioneered works³¹. In this study, an internal redistribution of only 10% of the trapped iodine in the first 2.5 cm of bed was observed after exposure of the silver zeolite to 1 MGy. The high stability of trapping in our case is due to the formation of AgI

in the course of I₂ adsorption. We can think that even if a small fraction of AgI formed could be oxidized with a potential release of I₂, the large excess of silver present in the porous material will trap again this fraction released.

On the other hand, the zeolite pre-irradiation (~ 2.2 MGy corresponding to ZEO2 test) did not induce any change in retention behavior, as compared with ZEO1. These results are consistent with the literature²¹, where no measurable change in adsorption efficiencies or in the microporous structure for zeolites after irradiation were observed. This was further confirmed in our recent study where the effect of pre-irradiation on the silver speciation of ion-exchanged zeolite was examined. XRD and DRS-UV-Vis did not reveal any change in the nature of silver species embedded in the pores.

4. CONCLUSION

In this paper, we aimed to investigate the I₂ retention behavior of some selected silver zeolites under a variety of conditions, including those which could be representative of a severe nuclear accident.

The adsorption characteristics of a dozen of different sorbents, containing different amounts of silver (0-35 wt%) and prepared from different structures (FAU X and Y, MOR, FER, *BEA, MFI), were first studied at 25°C in cyclohexane solvent. Adsorption capacities at saturation were found to depend much more on the silver content of the zeolites rather than on other zeolitic parameters such as the pore size or the pore connectivity. Adsorption kinetics follow a first or second order dependence towards the amount of free silver sites and the evidence of strong adsorption was confirming from the modeling of the I₂ adsorption isotherm and after-test characterization (AgI is the main adsorption product).

For the first time, a novel experimental setup was developed in order to study the I₂ dynamic retention behavior under flowing conditions at 100°C. Breakthrough profiles of some selected sorbents were obtained thanks to the online monitoring of I₂ concentrations by gas-phase UV-Vis spectroscopy. It was found that some exchanged faujasite zeolites (Y type) with 23 wt% silver have the best adsorption characteristics (more silver is not useful), with a usable working capacity of 330 mg/g and up to 80-85% of irreversible trapping (the other part being represented by physisorbed iodine). A pre-irradiation of silver zeolite (total dose 2.2 MGy) did neither change its physico-chemical characteristics nor its retention properties towards iodine. From the sorbent preparation viewpoint, the ion-exchange method could be preferred over impregnation because for the latter, kinetic limitations related to the solid-state diffusion of iodine in large silver nanoparticles may limit the storage of iodine as stable AgI precipitates. For a commercial Ag/X sorbent with 35 wt% silver, zeolite irradiation tests have shown that there is no measurable release of iodine after 30h of irradiation at 120°C in presence of wet air. Similar results were obtained after an additional pre-irradiation step (~ 2 MGy) of the zeolite before test. This confirms both the results of an ancient study and the high stability of AgI in accidental conditions. Although other zeolitic sorbents could be good candidates for a practical use in FCVS, it has to be ensured that the irreversible part of trapping is high. Such condition could be met in general for large-pore zeolites with high silver and low sodium contents.

ASSOCIATED CONTENT

Supporting Information

Photo of the EPICUR facility. Effect of preparation method and Si/Al ratio and of the irradiation on structural properties and silver speciation within Ag/Y zeolites. Experimental illustration by XRD of AgI formation after exposure to I₂ in liquid phase for the commercial sorbent (35Ag/13X_{comm} (1.2)). Description of the adsorption isotherms models. Summary on I₂ adsorption isotherm modeling (T=25°C, 35Ag/13X_{comm} (1.2)). Characterization of 4.2Ag/FER (10.4) zeolite before and after I₂ adsorption in liquid phase by DR-UV-Vis and XRD. XRD and DR-UV-Vis characterization of 22.8Ag/Y (2.5) and 23Ag/H-Y (40)_IWI after I₂ adsorption in gaseous phase ([I₂]₀=1250 ppm, T=100°C) (PDF)

AUTHOR INFORMATION

Corresponding Author

* E-mail: bruno.azambre@univ-lorraine.fr; Tel.: +33(0)372749856.

Present Addresses

- † IMT Atlantique (Mines Nantes), Energy and Environment Systems Department, Laboratoire GEPEA-UMR CNRS 6144, 4 Rue Alfred Kastler 44307 Nantes Cedex 3.

Author Contributions

- The manuscript was written through contributions of all authors. All authors have given approval to the final version of the manuscript.
- European Atomic Energy Community's (Euratom) Seventh Framework Programme FP7/2007-2013 (grant agreement n° 323217) ;
- National Research Agency ANR-MIRE (grant agreement n° ANR-11- RSNR-0013-01).

Notes

The authors declare no competing financial interest.

ACKNOWLEDGMENT

The research leading to these results is partly funded by the European Atomic Energy Community's (Euratom) Seventh Framework Programme FP7/2007-2013 under grant agreement n° 323217. This work has been also supported by the French State under the program "Investissements d'Avenir" called MIRE, managed by the National Research Agency (ANR) under grant agreement n° ANR-11-RSNR-0013-01.

REFERENCES

- (1) <https://gforge.irsn.fr/gf/project/passam/>.
- (2) <http://www.irsn.fr/EN/Research/Research-organisation/Research-programmes/MIRE-project/Pages/MIRE-project.aspx>.
- (3) Hidaka, A.; Yokoyama, H. Examination of ^{131}I and ^{137}Cs Releases during Late Phase of Fukushima Daiichi NPP Accident by Using $^{131}\text{I}/^{137}\text{Cs}$ Ratio of Source Terms Evaluated Reversely by WSPEEDI Code with Environmental Monitoring Data. *J. Nucl. Sci. Technol.* **2017**, *54* (8), 819.
- (4) Jacquemain, D.; Guentay, S.; Basu, S.; Sonnenkalb, M.; Lebel, L.; Allelein, H. J.; Liebana, B.; Eckardt, B.; Ammirabile, L. Status Report on Filtered Containment Venting; OECD/NEA/CSNI, Report NEA/CSNI/R (2014) 7, 2014.

- (5) http://www.aveva.com/globaloffer/liblocal/docs/Brochures/AREVA_Filtered-Containment-Venting-System_vEN.pdf
- (6) Herranz, L. E.; Lind, T.; Dieschbourg, K.; Riera, E.; Morandi, S.; Rantanen, P.; Chebbi, M.; Losch, N. State of the Art Report : Technical Bases for Experimentation on Source Term Mitigation Systems; Passam-Theor-T04 [D2.1], 2013.
- (7) Cantrel, L.; Herranz, L.; Guieu, S.; Albiol, T.; Collet, R.; Lind, T.; Kärkelä, T.; Mun, C.; Jacquemain, D.; Chebbi, M. Overview of Ongoing and Planned R&D Works on Delayed Radioactive Releases and Filtered Containment Venting Systems Efficiencies in a Severe Accident, Proceeding of ICAPP 2015, Nice, May 03-06, 2015.
- (8) Sava, D. F.; Chapman, K. W.; Rodriguez, M. A.; Greathouse, J. A.; Crozier, P. S.; Zhao, H.; Chupas, P. J.; Nenoff, T. M. Competitive I₂ Sorption by Cu-BTC from Humid Gas Streams. *Chem. Mater.* **2013**, *25* (13).
- (9) Nenoff, T. M.; Rodriguez, M. A.; Soelberg, N. R.; Chapman, K. W. Silver-Mordenite for Radiologic Gas Capture from Complex Streams: Dual Catalytic CH₃I Decomposition and I Confinement. *Microporous Mesoporous Mater.* **2014**, *200*, 297.
- (10) Chebbi, M.; Azambre, B.; Cantrel, L.; Koch, A. A Combined DRIFTS and DR-UV-Vis Spectroscopic in Situ Study on the Trapping of CH₃I by Silver-Exchanged Faujasite Zeolite. *J. Phys. Chem. C* **2016**, *120* (33), 18694.
- (11) Riley, B. J.; Vienna, J. D.; Strachan, D. M.; McCloy, J. S.; Jerden, J. L. Materials and Processes for the Effective Capture and Immobilization of Radioiodine: A Review. *J. Nucl. Mater.* **2016**, *470*, 307.

- (12) Sava Gallis, D. F.; Ermanoski, I.; Greathouse, J. A.; Chapman, K. W.; Nenoff, T. M. Iodine Gas Adsorption in Nanoporous Materials: A Combined Experiment-Modeling Study. *Ind. Eng. Chem. Res.* **2017**, acs. iecr.6b04189.
- (13) Chebbi, M.; Azambre, B.; Cantrel, L.; Huvé, M.; Albiol, T. Influence of Structural, Textural and Chemical Parameters of Silver Zeolites on the Retention of Methyl Iodide. *Microporous Mesoporous Mater.* **2017**, 244, 137.
- (14) Azambre, B.; Chebbi, M. Evaluation of Silver Zeolites Sorbents Towards Their Ability to Promote Stable CH₃I Storage as AgI Precipitates. *ACS Appl. Mater. Interfaces* **2017**, acsami.7b02366.
- (15) Jacobs, P. A.; Flanigen, E. M.; Jansen, J. C.; Bekkum, H. van. *Introduction to Zeolite Science and Practice*, 2th ed.; Elsevier sciences, 2001.
- (16) Thomas, T. R.; Staples, B. A.; Murphy, L. P.; Nichols, J. T. Airborne Elemental Iodine Loading Capacities of Metal Exchanged Zeolites and a Method for Recycling Silver Zeolites; Idaho National Engineering Laboratory: Idaho Falls, ID, 1977.
- (17) Brown, L. S. Chemistry: The Molecular Science, 2nd Edition (Olmsted, J. III; Williams, G.M.). *J. Chem. Educ.* **1998**, 75 (4), 419.
- (18) KAWAMURA, S.; KIMURA, T.; WATANABE, F.; HIRAO, K.; NARABAYASHI, T. Development of an Organic Iodine Filter for Filtered Containment Venting Systems of Nuclear Power Plants. *Trans. At. Energy Soc. Japan* **2016**, 15 (4), 192.
- (19) Burger, L. L.; Scheele, R. D.; Wiemers, K. D. Selection of a Form for Fixation of Iodine-129; PNL-4045/UC-70, Pacific Northwest Laboratory: Washington, 1981.

- (20) M Scheele, R. D ; Burger, L. L; Matsuzaki, C. L. Methyl Iodide Sorption by Reduced Silver Mordenite, PNL-4489/UC-70, Pacific Northwest Laboratory: Washington, 1983.
- (21) Pence, D. T.; Duce, F. A.; Maeck, W. J.; First, M. W. Developments in the Removal of Airborne Iodine Species with Metal Substituted Zeolites, Proceeding of the 12th AEC Air Cleaning Conference, Tennessee, Aug 28-31, 1972.
- (22) <http://www.cchem.com/zeolite/nuclear.html>.
- (23) Soelberg, N.; Watson, T. Iodine Sorbent Performance in FY 2012 Deep Bed Tests; INL/EXT-12-27075, Idaho National Laboratory: Idaho Falls, ID, 2012.
- (24) Sanemasa, I; Kobayashi, T; Piao, C.Y; Deguchi, T. Equilibrium Solubilities of Iodine Vapor in Water. *Bull. Chem. Soc. Jpn.* **1984**, *54*, 1352.
- (25) Payot, F; Devisme, F. Gaseous Iodine Trapping on Mineral Solid Filters : I-Isotherms and Kinetics, Atalante, Nîmes, June 21-25, 2004.
- (26) Chebbi, M. *Piégeage d'espèces iodées volatiles sur des adsorbants poreux de type zéolithique dans le contexte d'un accident nucléaire grave*, PhD thesis, University of Lorraine, october 2016.
- (27) Dushman, S. The Rate of the Reaction between Iodic and Hydriodic Acids. *J. Phys. Chem.* **1903**, *8* (7), 453.
- (28) Baker, M. D.; Ozin, G. A.; Godber, J. Far-Infrared Studies of Silver Atoms, Silver Ions, and Silver Clusters in Zeolites A and Y. *J. Phys. Chem.* **1985**, *89* (2), 305.
- (29) Sayah, E.; Brouri, D.; Massiani, P. A Comparative in Situ TEM and UV-visible

Spectroscopic Study of the Thermal Evolution of Ag Species Dispersed on Al₂O₃ and NaX Zeolite Supports. *Catal. Today* **2013**, 218–219, 10.

- (30) Falaise, C.; Volkringer, C.; Facqueur, J.; Bousquet, T.; Gasnot, L.; Loiseau, T.; Nenoff, T. M.; Shi, Z.; Feng, S. H.; Jonsson, M.; et al. Capture of Iodine in Highly Stable Metal–organic Frameworks: A Systematic Study. *Chem. Commun.* **2013**, 49 (87), 10320.
- (31) Evans, A.G. Radiation-Induced Iodine Migration in Silver Zeolites Beds, Proceeding of the 15^h AEC Air Cleaning Conference, Boston, Aug 7-10, 1978.